DOI: 10.1002/ejic.201000387

Synthesis and Electrical Capacitance of Carbon Nanoplates

Tao Mei,[a] Ting Li,[a] Huiyun Bi,[a] Liangbiao Wang,[a] Yongchun Zhu,*[a] and Yitai Qian*[a]

Keywords: Carbon / Nanoplates / Aggregation / Nanostructures / Capacitance properties

Carbon nanoplates with diameters and thicknesses of up to approximately 1.2 μm and 18 nm, respectively, were prepared by a reaction using CaC_2, ferrocene, and NH_4HCO_3 as starting materials at 600 °C for 10 h. These carbon nanoplates form aggregates that have a specific surface area of up to 831 $m^2 g^{-1}$ and a specific capacitance of up to 184 $F g^{-1}$ at a scanning rate of 10 $mV s^{-1}$ in a 3 $mol L^{-1}$ H_2SO_4 solution. Without using NH_4HCO_3, hexagonal carbon nanoplates with an average edge length of 500 nm and thickness of approximately 22 nm were obtained with a specific capacitance of up to 42 $F g^{-1}$. If NaN_3 or $NaHCO_3$ was used instead of NH_4HCO_3, carbon nanoplates with a curved surface or irregular circular carbon nanoplates were obtained with specific capacitances of 87 or 36 $F g^{-1}$, respectively.

Introduction

The electric double-layer capacitor (EDLC) using carbon materials as electrodes has been recognized as an efficient high-power energy device in electric power storage due to its better rate capability and longer cycle life relative to other capacitor materials.[1,2] The performance of carbon materials in EDLC depends on a number of factors, such as porosity,[3,4] specific surface area,[5,6] and structural order.[7–9] Two kinds of carbon materials, highly crystallized graphite and amorphous carbon, have been widely used as electrode materials in commercialized capacitors. Highly crystallized graphite has its advantage in its relatively low cost, high capacity, and flat discharge potential. However, the required temperature for preparation of highly crystallized graphite is usually above 2000 °C, which consumes a considerable amount of energy. In addition, the high-temperature graphitization process typically leads to a significant loss of specific surface area, resulting in low specific capacitance and energy density.[10] On the other hand, the preparation of amorphous carbon materials requires much lower temperature and less energy consumption. The carbonaceous material contains considerable hydrogen in C–H bonds and can uptake large quantities of ions; hence, it possesses very high capacity, while amorphous carbon has the disadvantage of considerable overvoltage or voltage loss.[11,12]

Recently, nanostructured carbon materials have been utilized as the electrode materials of capacitor devices. Nanostructured materials, which have large specific surface area and microporous structure, can greatly increase the electrode/electrolyte contact area, accommodate the structural deformation of the electrode, and shorten the diffusion path of current carriers.[13] Attention has been focused on nanostructured carbons, such as aerogels,[14–19] nanotubes,[20–24] nanotemplates,[25] and composites of carbon nanotubes and polymers.[26–28] 2D nanostructures have, in many cases, specific properties superior to those of 1D and 3D materials, and they have attracted great research interest due to their unique geometrical structure, mechanical properties, magnetic anisotropy, and excellent electrical properties.[29–31] It has been reported that nanostructured graphite plates can be used as good candidates for lightweight reinforcement,[32] emitters,[33] and catalyst support materials.[34] Nowadays, the synthesis of graphite plates is mainly limited by their intrinsic instability, as they have the notorious tendency to curve into tube structures or to stack by polarization interactions. 2D nanostructures of coin-like hollow carbon sheets,[34] two-layer-plane sheets,[35] graphite sheets,[31,36] and graphene[37,38] have been synthesized. Recently, flower-like carbon nanosheet aggregates with a specific surface area of 94 $m^2 g^{-1}$ were produced by a solvothermal technique at 800 °C, which exhibit a reversible capacity of 380 $mA h g^{-1}$ when they were applied as the anode in the charge/discharge experiments of secondary lithium ion batteries.[39] Carbon nanowalls on carbon cloth were obtained by using bias-assisted microwave plasma chemical vapor deposition in a CH_4/CO_2 system. They present a large specific surface area as high as 1580 $m^2 g^{-1}$ and a capacitance reaching up to approximately 198 $F g^{-1}$.[40] Carbon nanosheets that possess a capacitance of 0.076 $F cm^{-2}$ were coated on a conventional carbon paper or carbon fiber cloth by means of inductively coupled plasma (ICP)-enhanced chemical vapor deposition.[41] Studies of the graphene-based superca-

[a] Hefei National Laboratory for Physical Science at Microscale and Department of Chemistry,
University of Science and Technology of China,
Hefei, Anhui 230026, People's Republic of China
Fax: +86-551-360-7402
E-mail: ytqian@ustc.edu.cn
ychzhu@ustc.edu.cn

pacitor revealed that chemically modified graphene (CMG) could gain a capacitance as high as 135 $F g^{-1}$ in an aqueous solution.[42]

In this study, we demonstrate the synthesis of several kinds of carbon nanoplates. Aggregates of carbon nanoplates were prepared by a reaction using CaC_2, ferrocene, and NH_4HCO_3 as starting materials at 600 °C for 10 h. Hexagonal carbon nanoplates were synthesized from CaC_2 and ferrocene without the addition of NH_4HCO_3. If NaN_3 or $NaHCO_3$ was used to replace NH_4HCO_3, carbon nanoplates with a curved surface or irregular circular carbon nanoplates were obtained. Carbon nanoplates, which are assembled together to form aggregates, have surface areas of up to 831 $m^2 g^{-1}$. We also explored their electrochemical application as capacitor materials.

Results and Discussion

Figure 1a shows the typical XRD patterns of sample 1. The diffraction peak with a *d*-spacing of 3.374 Å can be indexed as the diffraction of the (002) plane of hexagonal graphite (JCPDS card no. 41-1487). Figure 1b shows the XRD patterns for sample 2 obtained without using NH_4HCO_3. The distinct diffraction peaks with *d*-spacing of 3.376, 2.041, and 1.682 Å can also be indexed as the diffractions of the (002), (101), and (004) planes, respectively, of hexagonal graphite (JCPDS card no. 41-1487).

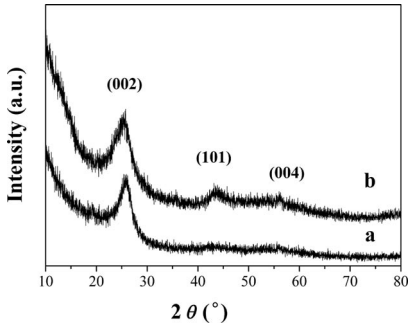

Figure 1. Typical XRD patterns of the products: (a) sample 1, (b) sample 2.

The representative Raman spectrum of sample 1 (Figure 2a) shows two obvious peaks at 1349 and 1586 cm^{-1}, which correspond to the D-band and G-band of graphite, respectively. The peak at 1586 cm^{-1}, named the G-band, corresponds to an E_{2g} vibration mode of graphite and is related to the vibration of sp^2-bonded carbon atoms in a 2D hexagonal lattice. The peak at 1349 cm^{-1}, named the D-band, is associated with the vibration of carbon atoms with dangling bonds of in-plane terminations of disordered graphite.[43] The peak shapes in the Raman spectrum of sample 2 (Figure 2b) are very similar to those of sample 1 but have different intensity. The smaller the intensity ratio of the D-band to the G-band (ID/IG) is, the higher the graphitization degree or the fewer the crystal defects.[44] The ID/IG values of sample 1 and sample 2 are 0.88 and 0.52, respectively, which indicates that the NH_4HCO_3 treatment increases the disorder and defects. Sample 2 exhibits higher graphitic degree than sample 1, while sample 2 has fewer defects than sample 1.

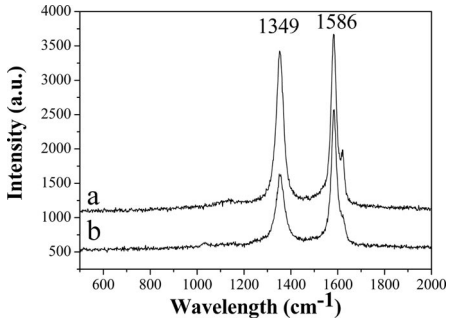

Figure 2. The typical Raman spectrum of the as-obtained products: (a) sample 1, (b) sample 2.

The morphologies and structures of the as-prepared samples were further analyzed by SEM and TEM. Figures 3a and b show typical SEM images of sample 1, in which a high proportion of carbon nanoplates is observed. Carbon nanoplates with diameters up to approximately 1.2 μm grow in an interlaced manner to form aggregates (Figure 3a). From the SEM (Figure 3b) and TEM images (Figure 3c), we can see that the thickness of the carbon nanoplates is approximately 18 nm. Moreover, they have smooth surfaces, uniform shapes, and a tendency to assemble together. Figure 3d shows the HRTEM image of sample 1. It clearly shows a layered but significantly disordered graphitic structure with an interlayer distance of 0.34 nm in some areas. The selected area electron diffraction (SAED) patterns of sample 1 are shown in the inset of Figure 3d. The inserted SAED patterns from innermost to the outermost correspond to the (002), (10), and (004) planes of hexagonal graphite. These result are consistent with those of XRD analysis.

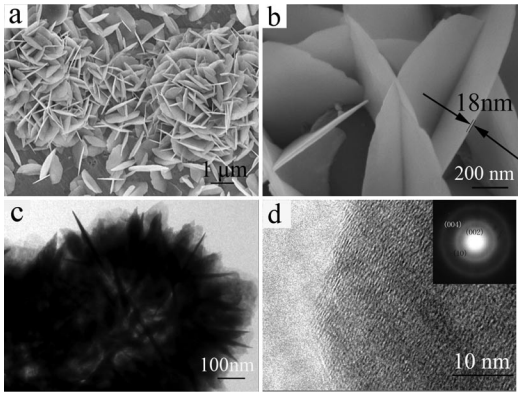

Figure 3. (a, b) Typical SEM images of sample 1. (c) TEM image of sample 1. (d) HRTEM image of sample 1. The inset is the SAED pattern of sample 1.

Interestingly, hexagonal carbon nanoplates were obtained in large quantities without the addition of NH_4HCO_3. The average edge length of sample 2 is 500 nm (Figure 4a), and the thickness of the wall is approximately 22 nm (Figure 4b). It is worth noting that the average thick-

ness value of sample 2 is greater than that of sample 1, whereas the diameter of sample 2 is smaller than that of sample 1. The texture of sample 2 with an edge length of approximately 500 nm can be clearly observed in the TEM images (Figure 4c). The HRTEM image of sample 2 (Figure 4d) was compared with the HRTEM image of sample 1, which indicates that sample 1 possesses a lower degree of graphitic crystallinity and more defects than sample 2. The result is consistent with the Raman spectroscopic data. The SAED patterns of sample 2 shown in the inset of Figure 4d are very similar to those of sample 1. The SAED patterns of sample 2 show a pair of small but strong arcs for the (002), together with a ring for the (101), and a pair of weak arcs for the (004) diffractions.

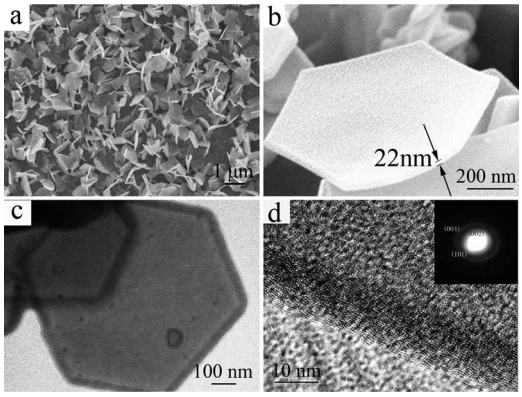

Figure 4. (a, b) Typical SEM images of sample 2. (c) TEM image of sample 2. (d) HRTEM image of sample 2. The inset is the SAED pattern of sample 2.

To analyze the morphology of the carbon nanoplates in detail, comparative experiments were carried out. Instead of NH_4HCO_3, 25 mmol NaN_3 or 18.75 mmol $NaHCO_3$ was used as starting material while keeping the other conditions unchanged. Carbon nanoplates with a curved surface were obtained by addition of NaN_3 as shown in Figure 5a. When $NaHCO_3$ was used, irregular circular carbon nanoplates were obtained (Figure 5b). We can conclude that the additive plays an important role in the morphology of nanoplates.

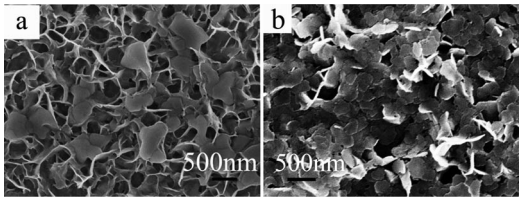

Figure 5. (a) Typical SEM images of sample 3 prepared by adding NaN_3 (25 mmol) and (b) sample 4 prepared by adding $NaHCO_3$ (18.75 mmol).

On the basis of experimental results, without the addition of NH_4HCO_3, the carbon atoms produced by the pyrolysis of CaC_2 and ferrocene form a carbon sheet with increasing reaction temperature. The carbon sheet grows to be hexagonal because of its intrinsic hexagonal phase with a space group of $P6_3/mmc$. When NH_4HCO_3 is added to this system, it decomposes into H_2O, CO_2, and NH_3, which provide a great deal of pressure up to approximately 134 atm and influence the crystal growth habit. It is reported that the momentary breakdown of the intercalates could play an important role in the forming process of the nanoplates.[45] It may be concluded that the NH_4HCO_3 treatment affects the morphology of the carbon nanoplates by increasing the disorder and defects, which are favorable for the deposition of carbon nanoplates, and the result can be confirmed by inspecting the Raman spectrum. In the process of NH_4HCO_3 treatment, some C–C bonds are broken while graphite layers with sp^2 structure begin to grow to form the carbon nanoplates. Ultimately, protuberant aggregates of carbon nanoplates are formed. The density of carbon nanoplates is related to the surface defects, which come from the NH_4HCO_3 treatment. The more defects there are, the easier aggregates of carbon nanoplates can form.[46]

Cyclic voltammetry (CV) measurements at various sweep rates (10–100 mV s^{-1}) were carried out in a 3 mol L^{-1} H_2SO_4 solution (Figure 6). The applied potentials were limited to values between –0.2 and 1.0 V (vs. SCE) to prevent the decomposition of water. The measured currents were converted into gravimetric single-electrode capacitances by normalizing with the electrode mass. The value of specific capacitance was determined by the equation $C = \Delta I/(2\upsilon m)$, where C is the specific capacitance, ΔI is the average current, υ is the voltage sweeping rate, and m is the mass of the active material in an electrode. Theoretically, an ideal CV curve of an electrochemical supercapacitor material should be of standard rectangular shape, since the capacitance C should keep constant at a linear charging/discharging rate (dV/dt = constant). The as-prepared carbon materials show good supercapacitive performance between –0.2 and 1.0 V (vs. SCE) and have approximately rectangular current–potential response curves. Herein anodic (oxidation) currents are given a negative sign, whereas cathodic (reduction) currents are given a positive sign. Figures 6a–e present the CV behavior of samples 1–4 and commercial lithium ion battery carbon material in a 3 mol L^{-1} H_2SO_4 solution. It could be observed that the CV curves of sample 1 at all the scanning rates were rectangle-shaped without obvious redox peaks (Figure 6a), which indicated ideal capacitive behavior and a very quick charging/discharging process.[47] However, sample 1 exhibits the best electrochemical performance relative to the other carbon products.

A mixed process, regardless of whether it involves a surface mechanism ($di/d\upsilon$ = constant = the capacitance) or a diffusion controlled mechanism ($di/d\upsilon^{1/2}$ = constant), can be simulated by the equation $C = k_1 + k_2/\upsilon^{1/2}$, from which k_1 and k_2 can be calculated if the plot of C vs. $\upsilon^{-1/2}$ is a straight line with slope k_2 and intercept k_1.[48] The slope is a measurement of the contribution of the diffusion process, so, at a low scan rate, the carbon materials can have more contact with the electrolytes, and then the diffusion process of inner surface contributes most of the capacitance. The specific capacitance values calculated from Figure 6 are presented in Figure 7. At a scanning rate of 10 mV s^{-1}, the spe-

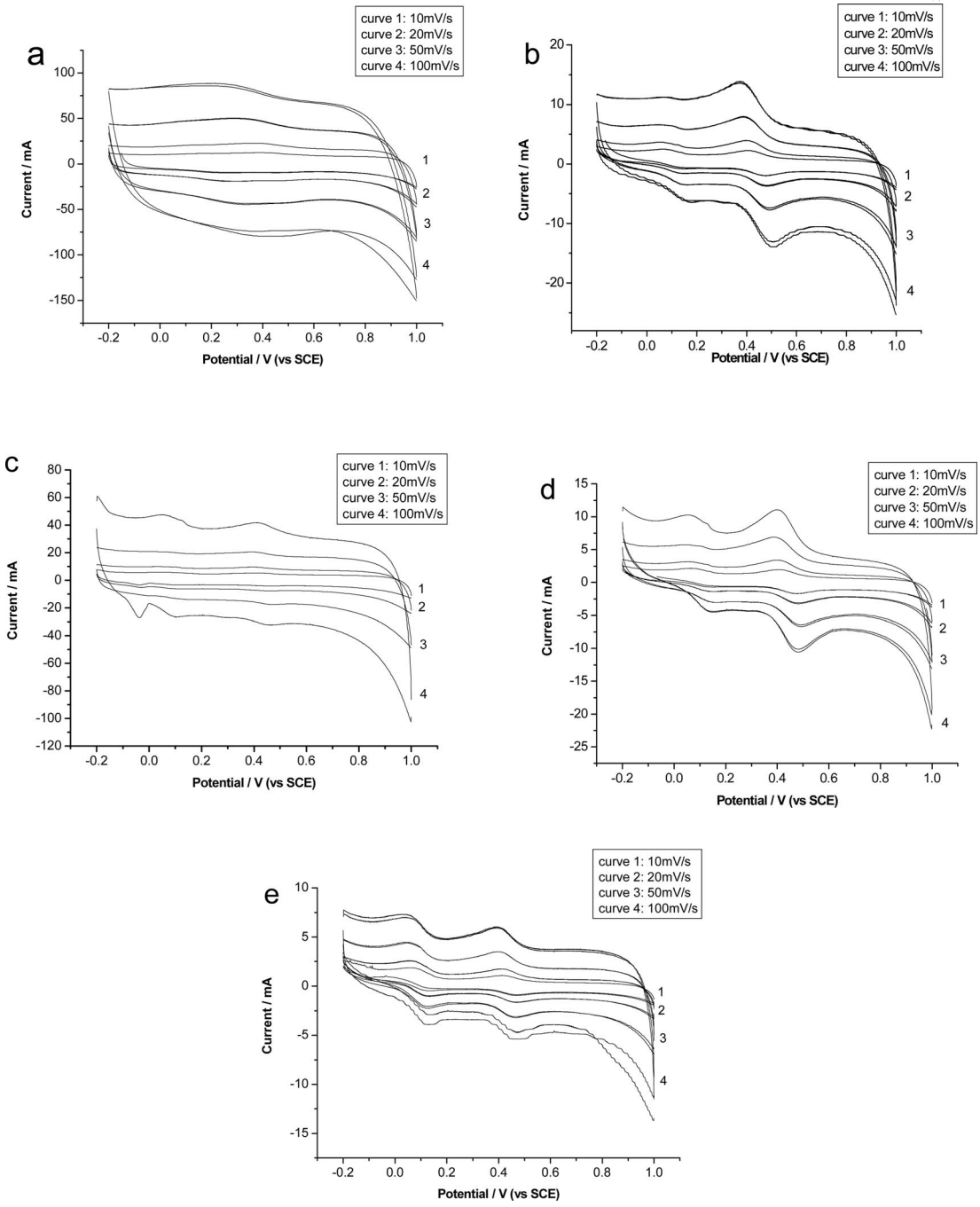

Figure 6. CV curves of sample 1 (a), sample 2 (b), sample 3 (c), sample 4 (d), and commercial lithium ion battery carbon material (e) at a scanning rate of 10 $mV\,s^{-1}$ (curve 1), 20 $mV\,s^{-1}$ (curve 2), 50 $mV\,s^{-1}$ (curve 3), and 100 $mV\,s^{-1}$ (curve 4) in a 3 $mol\,L^{-1}$ H_2SO_4 solution.

cific capacitances of sample 1, sample 2, sample 3, sample 4, and commercial lithium ion battery carbon material were 184, 42, 87, 36, and 32 $F\,g^{-1}$, respectively, whereas at a scanning rate of 100 $mV\,s^{-1}$, their specific capacitances were 132, 26, 70, 24, and 20 $F\,g^{-1}$, respectively. Obviously, at a high scan rate, the electrolyte can hardly be adsorbed on the surfaces of the carbon nanoplates. As a result, it cannot make full use of the inner surface area, which makes much contribution to the capacitance. The specific capacitance of sample 1 is about five times larger than that of the commercial lithium ion battery carbon materials due to the ease of penetration of the electrolyte into the gaps of the aggregates of carbon nanoplates.

The BET specific surface area and pore-size distribution of sample 1 were determined from the nitrogen adsorption/desorption isotherm (Figure 8), which exhibits type IV characteristics. The curve of sample 1 displays a hysteresis loop at a relative pressure (P/P_o) ≈ 0.4–1.0. The BET specific surface area of sample 1 is 831 $m^2\,g^{-1}$, which is much higher than that of previously reported natural graphite (1.7–6.0 $m^2\,g^{-1}$)[49] and expanded graphite (40–60 $m^2\,g^{-1}$).[50] It has been reported that an average pore size ranging from

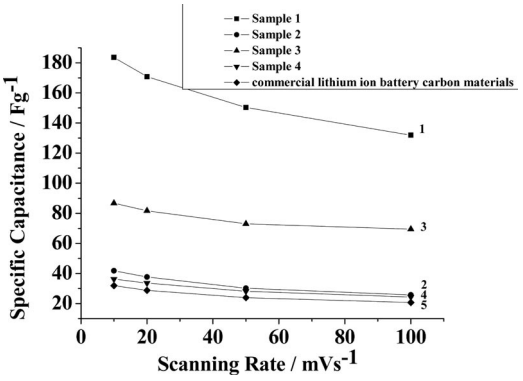

Figure 7. The specific capacitance of sample 1 (curve 1), sample 2 (curve 2), sample 3 (curve 3), sample 4 (curve 4), and commercial lithium ion battery carbon material (curve 5).

3 to 5 nm is believed to be most suitable for the penetration and adsorption of ions.[51] The inset of Figure 8 demonstrates that the pore-size distribution of sample 1 is concentrated at approximately 4 (peak 1) and 20 nm (peak 2). Peak 1 is attributed to the narrow interstices between the carbon nanoplates closing to the compact central part of the aggregate-like microstructure. The appearance of peak 2 is due to the thickness of the carbon nanoplates.

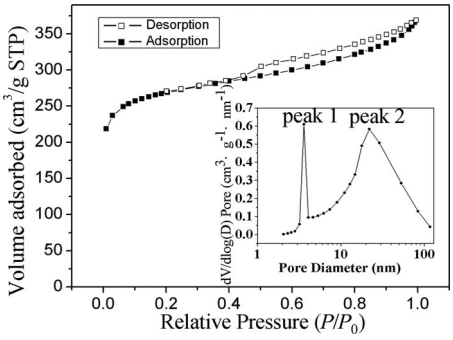

Figure 8. Nitrogen adsorption/desorption isotherm of sample 1. The inset shows the corresponding pore-size distribution curve calculated from the desorption branch by the Barrett–Joyner–Halenda method.

Due to residual surface "valencies", most carbon nanoplates that have been exposed to air contain adsorbed oxygen, which can lead to various O-based surface functionalities. Usually, these types of surface state could be modified by high-temperature treatment. The surface chemical properties of the as-prepared samples were further analyzed by XPS. The XPS spectrum of sample 1 (Figure 9) reveals evidence for the content of carbon, oxygen, and nitrogen species which are 93.02, 6.44, and 0.55 at.-%, respectively. For the purpose of comparison, Table 1 presents the surface chemical properties (XPS) and the BET specific surface area of all the carbon products. For carbon-based double-layer capacitors, the state of superficial oxidation especially at edge planes is of most significance. On one hand, this can determine the charge accommodation per gram and the corresponding capacitance. It can also influence the self-discharge characteristics of carbon capacitors. For such redox reactivity, a significant redox pseudocapacitance, C_Φ arises as well as the desired predominant double-layer capacity C_{dl}. In fact, for some carbon materials, it appears that C_Φ can amount to some 5–10% of the total realizable capacitance and scales approximately with the C_{dl} value. On the other hand, such surface structures influence the wettability of carbon materials, a matter of considerable importance in maximizing the access of electrolyte to the surface of carbon modifications in the preparation of electrochemical capacitor matrices.

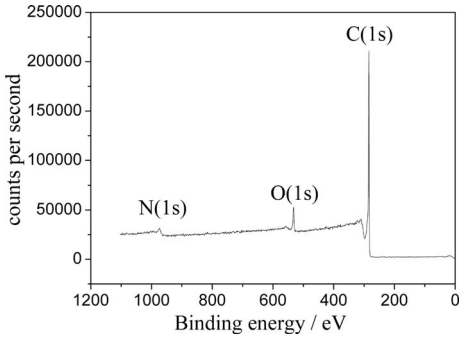

Figure 9. Typical XPS spectrum of sample 1.

Table 1. Surface chemical properties (XPS) and the BET specific surface area.

Sample	$C1s_{xps}$	$O1s_{xps}$	$N1s_{xps}$	$Na1s_{xps}$	BET ($m^2 g^{-1}$)
	(at.-%)				
1	93.02	6.44	0.55	0	831
2	99.64	0.36	0	0	57
3	87.34	11.14	0.28	1.23	104
4	97.70	1.02	0	1.28	17

Conclusions

We have prepared aggregates of carbon nanoplates with BET specific surface areas up to 831 $m^2 g^{-1}$ by using CaC_2, ferrocene, and NH_4HCO_3 as starting materials. Hexagonal graphite nanoplates were also obtained when NH_4HCO_3 was not added. As NaN_3 or $NaHCO_3$ was used to replace the NH_4HCO_3 as additive, carbon nanoplates with a curved surface or irregular circular carbon nanoplates were obtained. The factors influencing the structure and shape of the carbon products were investigated. The aggregates of carbon nanoplates have capacitances of up to 184 $F g^{-1}$ at a scanning rate of 10 $mV s^{-1}$.

Experimental Section

Preparation of Aggregates of Carbon Nanoplates: All the chemical reagents used here were of analytical grade and were used without further purification. In a typical synthesis process, ferrocene (3 mmol), CaC_2 powder (10 mmol), and NH_4HCO_3 (12.5 mmol) were mixed and placed in a stainless-steel autoclave of 20 mL capacity. The autoclave was sealed and put into an electronic furnace, which was heated from room temperature at 10 °C/min to 600 °C

and then maintained at 600 °C for 10 h. After that, the autoclave was cooled to room temperature naturally. In order to remove the byproducts, the precipitates in the autoclave were collected and washed with dilute hydrochloric acid, absolute ethanol, and distilled water several times. After that, the products were dried in vacuum at 60 °C for 5 h for further characterization and labeled as "sample 1".

Preparation of Hexagonal Carbon Nanoplates: For comparison, hexagonal carbon nanoplates were prepared by a reaction between ferrocene (3 mmol), and CaC_2 powder (10 mmol) without using NH_4HCO_3 while keeping the other conditions same. The products were labeled as "sample 2".

Preparation of Carbon Nanoplates with a Curved Surface: Carbon nanoplates with a curved surface were obtained by the reaction of NaN_3 (25 mmol), ferrocene (3 mmol), and CaC_2 (10 mmol), and the other conditions were unchanged. The products were labeled as "sample 3".

Preparation of Irregular Circular Carbon Nanoplates: Irregular circular carbon nanoplates were synthesized by the reaction of $NaHCO_3$ (18.75 mmol), ferrocene (3 mmol), and CaC_2 (10 mmol), and the other conditions were the same. The products were labeled as "sample 4".

Characterization

X-ray powder diffraction (XRD) patterns of the products were recorded with a Philips X′pert X-ray diffractometer with Cu-K_α radiation (λ = 1.54182 Å). The microstructure was observed with a transmission electron microscope (TEM, H7650), a high-resolution transmission electron microscope (HRTEM, JEOL-2010) with an accelerating voltage of 200 kV, and a field-emitting scanning electron microscope (SEM, JEOL-JSM-6700F). The Raman spectrum was recorded with a JY LABRAM-HR confocal laser micro-Raman spectrometer by using Ar^+ laser excitation with a wavelength of 514.5 nm. The Brunauer–Emmett–Teller (BET) surface area was measured with a Micromeritics ASAP 2020 accelerated surface area and porosimetry system. X-ray photoelectron spectra (XPS) were recorded with a VGESCA-LAB MKII X-ray photoelectron spectrometer, using non-monochromated Mg-K_α X-ray radiation as the excitation source.

The titanium sheets were previously etched by ultrasonic treatment in HCl solution (0.1 mol/L) at room temperature for 20 min to remove oxide layers, and then rinsed with doubly distilled water and dried in a vacuum oven at 373 K for 12 h. The electrode material was a mixture of carbon materials and poly(tetrafluoroethylene) with a mass ratio of 80:20. The solvent was dropped into the above mixture and ground to form the coating slurry. And this slurry was smeared onto the pretreated titanium sheet that served as current collector, and then the electrode was dried in a vacuum oven at 423 K for 2 h. The electrochemical performance was investigated by using cyclic voltammetry (CV) in a standard three-electrode cell kept at 25 °C by means of a water bath. CV experiments in a H_2SO_4 solution (3 mol L^{-1}) were performed with a CHI 660D electrochemical workstation. A platinum foil was used as counterelectrode. All potentials were measured with reference to a saturated calomel electrode (SCE). The specific capacitance of the electrode can be calculated by plotting CV capacity vs. electrode potential and tracing the regression line. The slope of this line gives the specific capacitance, which is based on the mass of the electroactive materials in the electrodes. The scan rates of CV tests were adjusted from 10 to 100 mV s^{-1}.

Acknowledgments

The financial support of this work by the 973 Project of China (No. 2005CB623601) is gratefully acknowledged.

[1] A. Nishino, *J. Power Sources* **1996**, *60*, 137–147.
[2] T. Christen, M. W. Carlen, *J. Power Sources* **2000**, *91*, 210–216.
[3] E. Frackowiak, F. Beguin, *Carbon* **2001**, *39*, 937–950.
[4] S. Shiraishi, H. Kurihara, H. Tsubota, A. Oya, Y. Soneda, Y. Yamada, *Electrochem. Solid State Lett.* **2001**, *4*, A5–A8.
[5] D. Y. Qu, H. Shi, *J. Power Sources* **1998**, *74*, 99–107.
[6] J. Gamby, P. L. Taberna, P. Simon, J. F. Fauvarque, M. Chesneau, *J. Power Sources* **2001**, *101*, 109–116.
[7] H. Yang, M. Yoshio, K. Isono, R. Kuramoto, *Electrochem. Solid State Lett.* **2002**, *5*, A141–A144.
[8] Y. J. Kim, Y. Horle, Y. Matsuzawa, S. Ozaki, M. Endo, M. S. Dresselhaus, *Carbon* **2004**, *42*, 2423–2432.
[9] M. Toyoda, Y. Tani, Y. Soneda, *Carbon* **2004**, *42*, 2833–2837.
[10] M. Winter, J. O. Besenhard, M. E. Spahr, P. Novak, *Adv. Mater.* **1998**, *10*, 725–763.
[11] M. Noel, V. Suryanarayanan, *J. Power Sources* **2002**, *111*, 193–209.
[12] H. L. Zhang, S. H. Liu, F. Li, S. Bai, C. Liu, J. Tan, H. M. Cheng, *Carbon* **2006**, *44*, 2212–2218.
[13] G. F. Zou, D. W. Zhang, C. Dong, H. Li, K. Xiong, L. F. Fei, Y. T. Qian, *Carbon* **2006**, *44*, 828–832.
[14] Y. Z. Wei, B. Fang, S. Iwasa, M. Kumagai, *J. Power Sources* **2005**, *141*, 386–391.
[15] J. W. Long, B. M. Dening, T. M. McEvoy, D. R. Rolison, *J. Non-Cryst. Solids* **2004**, *350*, 97–106.
[16] S. W. Hwang, S. H. Hyun, *J. Non-Cryst. Solids* **2004**, *347*, 238–245.
[17] W. C. Li, H. Probstle, J. Fricke, *J. Non-Cryst. Solids* **2003**, *325*, 1–5.
[18] H. Talbi, P. E. Just, L. H. Dao, *J. Appl. Electrochem.* **2003**, *33*, 465–473.
[19] R. W. Pekala, J. C. Farmer, C. T. Alviso, T. D. Tran, S. T. Mayer, J. M. Miller, B. Dunn, *J. Non-Cryst. Solids* **1998**, *225*, 74–80.
[20] H. S. Ye, X. Liu, H. F. Cui, W. D. Zhang, F. S. Sheu, T. M. Lim, *Electrochem. Commun.* **2005**, *7*, 249–255.
[21] C. Emmenegger, P. Mauron, P. Sudan, P. Wenger, V. Hermann, R. Gallay, A. Zuttel, *J. Power Sources* **2003**, *124*, 321–329.
[22] B. Zhang, J. Liang, C. L. Xu, B. Q. Wei, D. B. Ruan, D. H. Wu, *Mater. Lett.* **2001**, *51*, 539–542.
[23] E. Frackowiak, K. Jurewicz, S. Delpeux, F. Beguin, *J. Power Sources* **2001**, *97–8*, 822–825.
[24] K. H. An, W. S. Kim, Y. S. Park, Y. C. Choi, S. M. Lee, D. C. Chung, D. J. Bae, S. C. Lim, Y. H. Lee, *Adv. Mater.* **2001**, *13*, 497–500.
[25] P. A. Nelson, J. R. Owen, *J. Electrochem. Soc.* **2003**, *150*, A1313–A1317.
[26] F. Beguin, K. Szostak, G. Lota, E. Frackowiak, *Adv. Mater.* **2005**, *17*, 2380–2384.
[27] V. Khomenko, E. Frackowiak, F. Beguin, *Electrochim. Acta* **2005**, *50*, 2499–2506.
[28] T. V. Sreekumar, T. Liu, B. G. Min, H. Guo, S. Kumar, R. H. Hauge, R. E. Smalley, *Adv. Mater.* **2004**, *16*, 58–61.
[29] Y. H. Leng, Y. Li, X. G. Li, S. Takahashi, *J. Phys. Chem. C* **2007**, *111*, 6630–6633.
[30] L. M. Viculis, J. J. Mack, O. M. Mayer, H. T. Hahn, R. B. Kaner, *J. Mater. Chem.* **2005**, *15*, 974–978.
[31] J. J. Wang, M. Y. Zhu, R. A. Outlaw, X. Zhao, D. M. Manos, B. C. Holloway, V. P. Mammana, *Appl. Phys. Lett.* **2004**, *85*, 1265–1267.
[32] J. J. Mack, L. M. Viculis, A. Ali, R. Luoh, G. L. Yang, H. T. Hahn, F. K. Ko, R. B. Kaner, *Adv. Mater.* **2005**, *17*, 77–80.
[33] J. Y. Wang, T. Ito, *Diam. Relat. Mater.* **2007**, *16*, 589–593.

[34] D. S. Yuan, C. W. Xu, Y. L. Liu, S. Z. Tan, X. Wang, Z. D. Wei, P. K. Shen, *Electrochem. Commun.* **2007**, *9*, 2473–2478.
[35] Y. Xiao, Y. L. Liu, D. S. Yuan, *Carbon* **2008**, *46*, 559–561.
[36] J. J. Wang, M. Y. Zhu, R. A. Outlaw, X. Zhao, D. M. Manos, B. C. Holloway, *Carbon* **2004**, *42*, 2867–2872.
[37] D. W. Wang, F. Li, Z. S. Wu, W. C. Ren, H. M. Cheng, *Electrochem. Commun.* **2009**, *11*, 1729–1732.
[38] M. Choucair, P. Thordarson, J. A. Stride, *Nat. Nanotechnol.* **2009**, *4*, 30–33.
[39] J. M. Shen, Y. T. Feng, *J. Phys. Chem. C* **2008**, *112*, 13114–13120.
[40] T. C. Hung, C. F. Chen, W. T. Whang, *Electrochem. Solid State Lett.* **2009**, *12*, K41–K44.
[41] X. Zhao, H. Tian, M. Y. Zhu, K. Tian, J. J. Wang, F. Y. Kang, R. A. Outlaw, *J. Power Sources* **2009**, *194*, 1208–1212.
[42] M. D. Stoller, S. J. Park, Y. W. Zhu, J. H. An, R. S. Ruoff, *Nano Lett.* **2008**, *8*, 3498–3502.
[43] D. G. Mcculloch, S. Prawer, A. Hoffman, *Phys. Rev. B* **1994**, *50*, 5905–5917.
[44] H. B. Li, Y. C. Zhu, Z. H. Mao, J. Gu, J. H. Zhang, Y. T. Qian, *Carbon* **2009**, *47*, 328–330.
[45] G. L. Sun, X. J. Li, Y. D. Qu, X. H. Wang, H. H. Yan, Y. J. Zhang, *Mater. Lett.* **2008**, *62*, 703–706.
[46] L. Y. Zeng, D. Lei, W. B. Wang, J. Q. Liang, Z. Q. Wang, N. Yao, B. L. Zhang, *Appl. Surf. Sci.* **2008**, *254*, 1700–1704.
[47] S. Ghosh, O. Inganas, *Adv. Mater.* **1999**, *11*, 1214–1218.
[48] T. C. Liu, W. G. Pell, B. E. Conway, S. L. Roberson, *J. Electrochem. Soc.* **1998**, *145*, 1882–1888.
[49] Y. Sato, R. Hagiwara, Y. Ito, *Solid State Sci.* **2003**, *5*, 1285–1290.
[50] A. Celzard, J. F. Mareche, G. Furdin, *Carbon* **2002**, *40*, 2713–2718.
[51] K. H. An, W. S. Kim, Y. S. Park, J. M. Moon, D. J. Bae, S. C. Lim, Y. S. Lee, Y. H. Lee, *Adv. Funct. Mater.* **2001**, *11*, 387–392.

Received: April 8, 2010
Published Online: August 18, 2010

